

# 9

## Catalysis by Metal and Oxide Nanoparticles, Single Metal Atoms and Di-Nuclear Oxo-Ions in Zeolites

Wolfgang M. H. Sachtler

### 9.1. INTRODUCTION

Nanoparticles of precious metals have been routinely used in heterogeneous catalysis for more than half a century. Zeolites with a well-defined regular network of nanopores and nanocages were introduced by the Mobil company in 1964<sup>1</sup> because their superior acidity enables them to better catalyze hydrocarbon conversions involving carbenium ion intermediates, such as isomerization, dehydrocyclization, and cracking. The high acidity of zeolites in their H-form is a consequence of their structure: As shown by van Santen *et al.*, the energy required to remove a proton from an OH-group is lower if flexibility of the lattice accommodates the charge of the resulting O<sup>-</sup> ion.<sup>2</sup> Unusual stereoselectivity in alkylation of aromatic molecules has been achieved by Csicsery with acid zeolites, because these solids act as molecular sieves, favoring diffusion of small linear molecules over that of more bulky or branched isomers. In addition, the finite volume of nanocages in zeolites favors transition states which are compatible with the cage dimensions.<sup>3</sup> A well-known process exploiting this feature is the methanol-to-gasoline process which converts methanol to high octane gasoline over an acid zeolite

---

Department of Chemistry and Institute for Environmental Catalysis, Northwestern University, Evanston, IL; E.mail: wmhs@northwestern.edu

of MFI structure. While acid catalyzed polymerization and dehydro-condensation can produce unsaturated olefins or aromatic compounds of any size, the pores in the MFI framework limit this process to products of the size of tetra-methyl benzene.

The use of very small metal particles in supported catalysts is now common industrial practice. More recently, it has been found that catalytic oxidation of organic molecules is highly selective over catalysts that expose small oxo-ions of a transition metal rather than multiatomic oxide particles.<sup>4</sup> This chapter will focus on supported metal catalysts and zeolite-supported transition metal oxides. The fundamental principles which distinguish the catalytic propensities of these systems from those of their macroscopic counterparts will be sketched and illustrated by a few examples. The techniques used to prepare such catalysts and protect nano- and subnano particles against agglomeration will be described. Extreme examples of heterogeneous catalysts with nanoparticle sites are a Pt/mordenite catalyst exposing isolated Pt atoms and an Fe/MFI catalyst with oxo-ions as the sites catalyzing oxidation.

## 9.2. SUPPORTED METAL CLUSTERS

A crucial invention was made in 1947 by V. Haensel and his associates at Universal Oil Products. They developed a catalyst for the conversion of predominantly straight chain paraffinic hydrocarbons to high octane gasoline.<sup>5</sup> Their catalyst converted 90% of a low octane gasoline into a product with an octane rating above 80 and had an astonishingly long life. The support was alumina; presumably this was the first bifunctional catalyst, exposing both platinum atoms and acid sites. It was soon found that performance could be substantially improved by chemical treatments that produce even stronger acidic sites on the alumina.

Using a catalyst with an expensive metal for producing a cheap commodity challenged conventional economic wisdom. (The price of gasoline in the United States was roughly 8¢ per gallon at the time). It was demonstrated that long life and *in situ* regeneration of the catalyst justify a high initial price. To keep that price within acceptable limits, it was crucial to minimize the amount of platinum by maximizing its dispersion. The Pt content of the catalyst was 0.1%. Hydrogen adsorption indicated that 50% or more of the Pt atoms were surface atoms. The inventors coined the new word “platforming” for the new process. The term “nanoparticle” did not yet exist.

High metal dispersion results in exposure of metal sites of enhanced catalytic activity. I. Stranski *et al.* used the Gibbs–Wulff principle<sup>6–8</sup>

$$\Sigma(\sigma_{hkl}A_{hkl}) = \text{Minimum} \quad [\sigma = \text{specific surface energy; } A = \text{surface area}] \quad (1)$$

to estimate the equilibrium shape of metal crystals and showed not only, why polyhedra are formed with atomically close-packed crystal faces, but also that with metals the sharp edges and corners of perfect polyhedra will be blunted, so that segments of less stable crystal faces become exposed. Regions of “blunted” edges and corners expose coordinatively unsaturated metal atoms. Such crystallographical regions have a lower electronic work function than close-packed crystal faces; the first evident confirmation of Stranski’s conclusions was provided by the invention of the field emission microscope. This instrument uses electron emission from the sharp tip of a needle-shaped emitter; the bright regions in the resulting image clearly show the presence of atomically

“open” faces. Moreover, electron microscopic images of such tips show their edge-less and corner-less shape in contrast to the polyhedra of macroscopic crystals.

The difference between the close-packed crystal faces, such as (110) in bcc or (111) in fcc crystals, and the “open” faces that prevail in the surface of nano particles, is of relevance to heterogeneous catalysis, because most adsorbates are more strongly bonded to the “coordinatively unsaturated” metal atoms in the “open” faces.

Sabatier and Balandin had predicted a relationship between catalytic activity and heat of adsorption. If a solid adsorbs the reactants only weakly, it will be a poor catalyst, but if it holds reactants, intermediates or products too strongly, it will again perform poorly. The ideal catalyst for a given reaction was predicted to be a compromise between too weak and too strong chemisorption. Balandin transformed this concept to a semiquantitative theory by predicting that a plot of the reaction rate of a catalytic reaction as a function of the heat of adsorption of the reactant should have a sharp maximum. He called these plots “volcano-shaped curves.”<sup>9</sup> This prediction was confirmed by Fahrenfort *et al.*<sup>10,11</sup> An example of their “volcano-shaped curve” is reproduced in Fig. 9.1. They chose the catalytic decomposition of formic acid

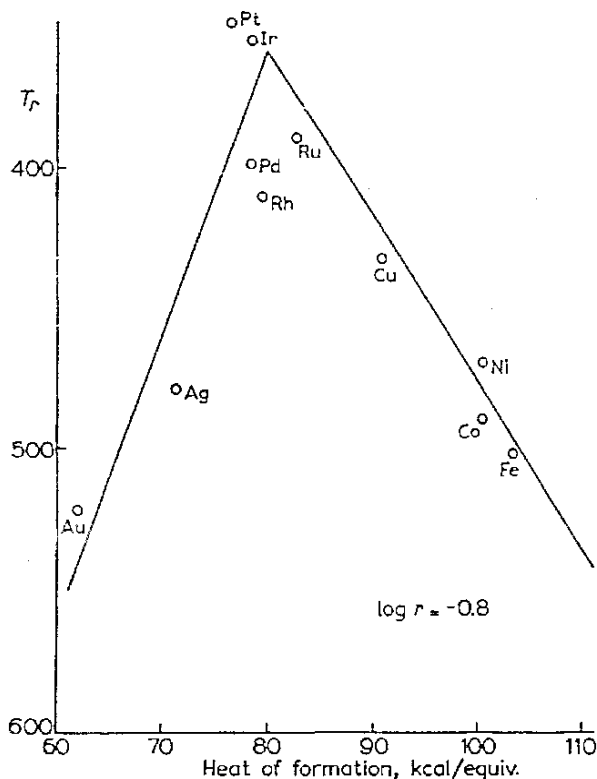
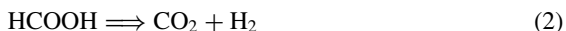


FIGURE 9.1. “Volcano Plot” of formic acid decomposition. Abscissa: Calculated  $\Delta H_{ads}$  of HCOOH; Ordinate: Temperature at which rate of HCOOH decomposition reaches the same value for all metals.

as the probe reaction, because it is catalyzed by a large number of metals, including gold and silver on the ascending branch of the volcano, while iron and tungsten with high heats of chemisorption are located on the descending branch of the plot. Although Fig. 9.1 has been reproduced in review papers and textbooks, a short explanation might be useful.

There were not many calorimetric data on the heat of adsorption available at the time of its first publication in 1959. However, the data that were available showed that enthalpies of chemisorption,  $\Delta H_{\text{ads}}$ , tend to be proportional to the enthalpies of formation of the enthalpies of formation of the corresponding bulk compounds,  $\Delta H_{\text{form}}$ ; moreover the heats of formation of oxides, nitrides, hydrides and formates are, in first approximation, proportional to each other. When only a relative ranking of metals is required as is the case with Balandin's theory, it is permitted to make use of these relationships where no direct calorimetric data are available. A second remark pertains to the measured catalytic activity. As the reaction rates differ by several orders of magnitude between the most active metals at the top of the volcano and the least active ones at the two feet, most authors who measure catalytic rates use equipment optimized for a certain range of reaction rates and adjust the temperature of the catalyst accordingly. In order to avoid risky extrapolations from the measured data, we decided not to plot the rate at a given temperature, but the temperature at which a given rate was attained. As the most active catalyst attains this prefixed rate at a lower temperature than a poor catalyst, the concept is best illustrated by using an inverted linear temperature scale at the ordinate axis of Fig. 9.1, so that the most active catalyst will appear at the top of the volcano.

Upon considering that heats of chemisorption will generally be higher on nanocrystals than on metals in their macroscopic form, this concept leads to two consequences:

- (1) For the metals on the left leg of the volcano plot, an increase of the heat of adsorption will ensue enhanced catalytic activity. This consequence applies most obviously to gold which in its standard state is a poor catalyst because heats of adsorption of most molecules are very low on gold. Indeed, Haruta and other authors confirmed that gold becomes very active when present as nanoparticles.<sup>12</sup>
- (2) For the metals on the right leg of the volcano plot, where heat of adsorption is high, the surface structure is no longer that of the stable polyhedron under vacuum as considered in the calculations by Stranski *et al.* In 1966 Holscher and Sachtler showed that strong chemisorption is *corrosive*, which means that surface atoms leave their original positions and arrange themselves with the adsorbed entities to a two-dimensional compound.<sup>13</sup> This phenomenon, later called *surface reconstruction*, has been confirmed for a large number of metal/adsorbate systems.

The heat of chemisorption is, of course, the energy difference between the chemical bonds formed and those broken. One of the strongest bonds to be broken in dissociative chemisorption on metals is the N–N bond of  $\text{N}_2$ . This chemisorption is known to be rate limiting in ammonia synthesis. Brill *et al.* reported in 1967 field emission results indicating that  $\text{N}_2$  adsorption on Fe is strongest on the (111) face.<sup>41</sup> Their suspicion that this might be the initial step in ammonia synthesis over Fe catalysts

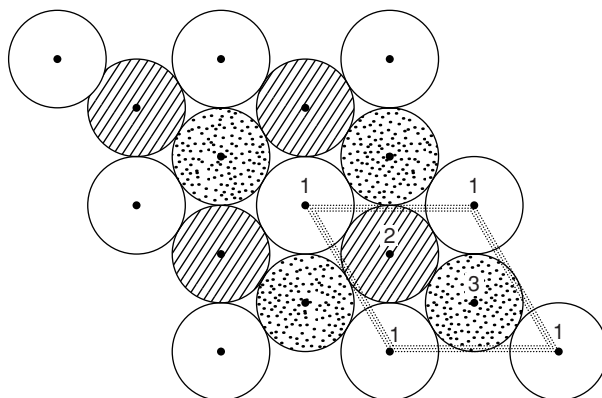


FIGURE 9.2. Surface topography of (111) face of bcc metal with probable sites for dissociative chemisorption of  $N_2$  on bcc Fe.

was confirmed by H. Topsøe who showed that the measured synthesis activity correlates with the area of the (111) face.<sup>14</sup> Inspecting the microtopography of this crystal face reveals that the outermost Fe atoms are widely spaced creating hollow sites of 6 Fe atoms located in three parallel (111) planes, as illustrated in Fig. 9.2. It stands to reason that these are the sites where  $N_2$  molecules are dissociatively chemisorbed. The ammonia synthesis is thus another example for a catalytic reaction depending on crystal faces with a very open structure. This illustrates the need for surface science to focus on nanoparticles, because the atomically close-packed faces that prevail on macroscopic metal crystals are of limited relevance to heterogeneous catalysis.

### 9.3. CHEMICAL ANCHORING AND DE-ANCHORING

For metal atoms the state of lowest Gibbs Free Energy is achieved when they are organized in a macroscopic polyhedron. High dispersion on a support requires strong chemical interaction between metal and support, conventionally called “*chemical anchoring*.” The formation of solid particles either from the vapor or from an adsorbed precursor is dominated by two kinetic processes:

- (1) Nucleation
- (2) Growth

The interplay of these two basic rates determines the size of the resulting particles. For instance, the reason that snow flakes reach sizes of several cm at lower latitudes but arrive as extremely small crystals, called “diamond dust” in Antarctica, is that the nuclei that are formed in a cloud, will grow during their voyage to earth by adsorbing water molecules. Obviously, this growth will be more important in the moist atmosphere at low latitudes than in the extremely dry atmosphere above Antarctica. The same interplay of nucleation and growth determine the size of metal particles that are formed on a support by chemical reduction of adsorbed precursors, such as metal ions. Here

the rate of growth of the nuclei is determined by the transport of the precursor ions over the surface of the support. Fully ligated metal ions are usually quite mobile at moderate temperatures, but if ligands and surface hydroxyl groups are removed by thermal treatment, the oxide ions of the support surface will act as ligands to the adsorbed metal ions and slow down its movements. Needless to say, very small metal particles will be obtained if the rate of nucleation is large and the rate of growth is small.

As an aside, we should mention that the same principles apply to the formation of bimetallic clusters on a support. In the case of Pt–Re on  $\text{Al}_2\text{O}_3$  it has been shown that hydroxylation of the surface favors the ability of Re ions to migrate toward the Pt nuclei and thus the formation of alloy particles, whereas fixing the Re ions onto a dehydroxylated alumina surface creates mainly separated Re particles. As catalytic activity and selectivity of the bimetallic particles differ vastly from those of a physical mixture of monometallic particles, the catalytic performance of the reduced catalyst depends significantly on the protocol used during its formation.<sup>15–17</sup> The bimetallic Pt–Re catalysts have been identified by comparison with preparations in which gaseous Re carbonyl was decomposed on conventionally prepared Pt/ $\text{Al}_2\text{O}_3$  catalysts.<sup>18</sup>

Chemical anchoring of catalytically active metal clusters onto a support is of practical importance to stabilize catalysts against loss of activity by *Ostwald ripening*, i.e. metal agglomeration. Documented examples include Pt, Pd, or Rh supported on acidic oxides, in particular zeolites in their H-form.<sup>19–22</sup> Three types of anchors have been described in the literature: (a) Brønsted acid sites, (b) Lewis acid sites, (c) transition metal ions. The interaction of metal atoms with a strong Brønsted acid site leads to formation of proton–metal adducts that are of importance in bifunctional catalysts, such as Pt, Pd, or Rh supported on an acidic oxide, in particular a zeolite in its acidic form.<sup>23–25</sup> Recently, Zhang *et al.* have reported on hydrodechlorination of  $\text{CCl}_4$  over Pt/ $\text{Al}_2\text{O}_3$  catalysts.<sup>22</sup> Whereas Pt nanoparticles deactivate rapidly due to HCl poisoning, larger Pt particles are remarkably stable. Controlled agglomeration of primary nanoclusters to stable particles was achieved in an atmosphere of  $\text{NH}_4\text{Cl}$ . The mechanism of this controlled growth is ascribed to de-anchoring by Cl adsorption of the Pt clusters.

De-anchoring is understood as the action of an adsorbate that forms a chemical bond with a surface metal atom that is stronger than the bond which held this metal atom when anchored to its site. This phenomenon has been demonstrated with palladium atoms that were held onto the cage walls of a Y zeolite as palladium proton adducts. Once this system was exposed to carbon monoxide, Pd formed Pd–CO bonds that are much stronger than the original Pd–H bonds. As a result, the Pd–CO complex become mobile at low temperature and will oligomerize with other Pd–CO entities to Pd carbonyl clusters.<sup>26</sup> These are identified by their very characteristic IR spectrum with C–O vibrations giving much sharper IR bands than those usually observed with CO on Pd or other supported transition metals. Figure 9.3 shows an example.

The identification of these carbonyl clusters was achieved by comparison with the spectra of  $\text{Pd}_{13}(\text{CO})_n$  clusters that have been unambiguously characterized by XRD and other techniques. As the IR bands can be assigned to linear, bridging and triple-bridging CO it is assumed that the carbonyl cluster responsible for the spectrum in Fig. 9.3 has a core of 13 Pd atoms of icosahedral structure. Interestingly, these neutral complexes can only be observed in zeolite cages, where they are entrapped inside cages which prevent their agglomeration to larger clusters. Both the size of the cage and the width of the windows are essential for the (meta-) stability of these compounds. Spectra obtained

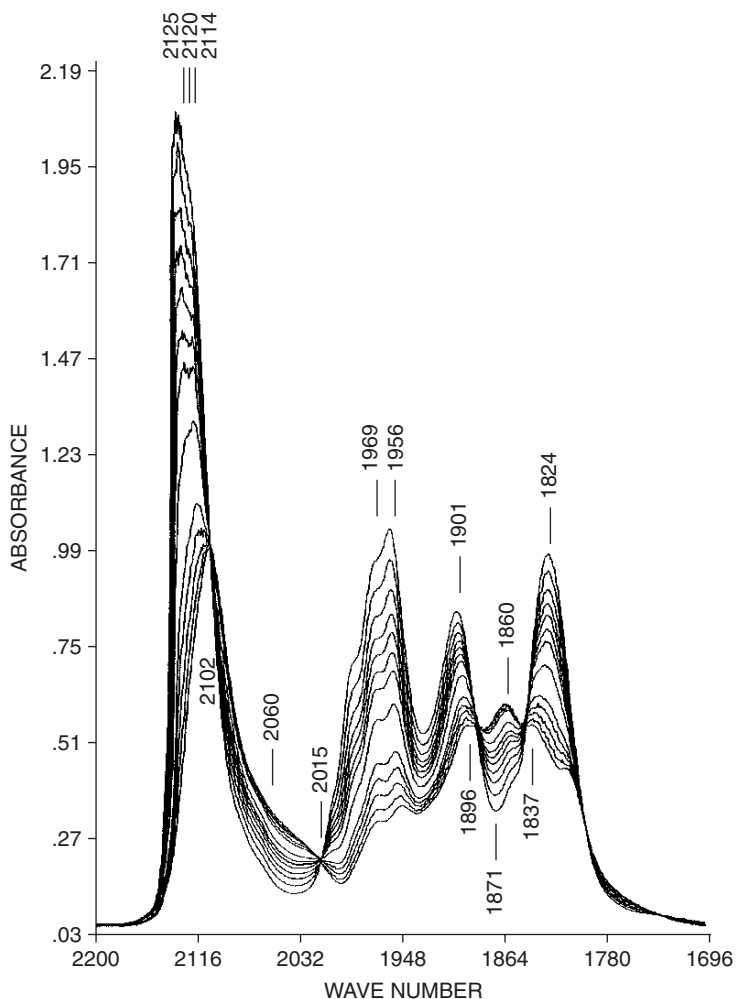


FIGURE 9.3. FTIR spectrum of Pd carbonyl cluster in zeolite cages.

after exposure to higher temperature, form larger Pd particles, positioned outside the zeolite cages and more reminiscent of the IR spectral normally obtained with CO on less well-defined Pd clusters.

#### 9.4. MONOATOMIC PLATINUM IN ZEOLITES

The extreme case of an ultrananostructure consists of one single atom. Such monoatomic Pt sites have been realized in Pt/H-zeolites that are prepared at low temperature. They are identified by their unique selectivity in catalyzing the H/D exchange between cyclopentane and D<sub>2</sub>. Numerous data in the literature show that over conventional Pt

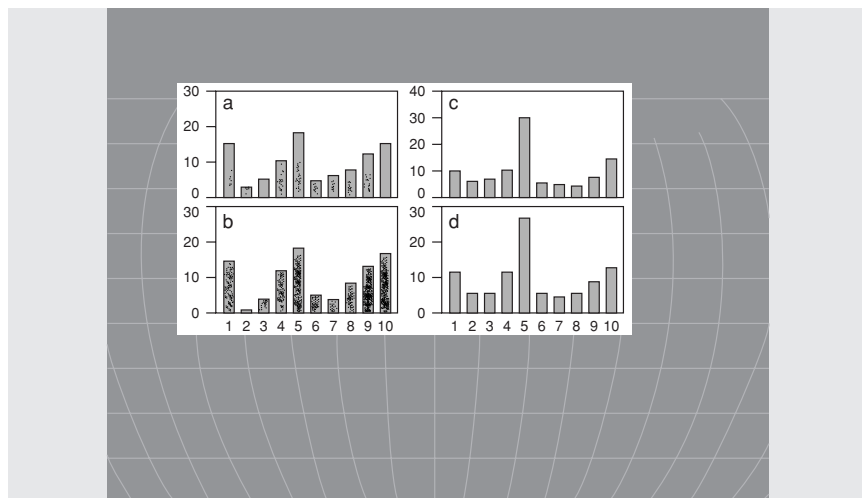


FIGURE 9.4. Distribution patterns of deuterium cyclopentanes Multiple exchange after H/D exchange over conventional Pt catalysts with Pt<sub>n</sub> particles. Abscissa: Value of  $x$  in C<sub>5</sub>H<sub>(10-x)</sub>D<sub>x</sub> fraction; ordinate: rel. abundance.

catalysts, exposing multiatomic Pt<sub>n</sub> sites, this reaction follows the “multiple-exchange” pathway, i.e. more than one H atom of cyclopentane is exchanged during a residence of the molecule on a Pt<sub>n</sub> site. All five H atoms at the same side of the C<sub>5</sub> ring can be easily exchanged while the molecule is adsorbed. In the presence of an excess of D<sub>2</sub> this leads to the preferential formation of C<sub>5</sub>H<sub>5</sub>D<sub>5</sub>.<sup>27–29</sup>

Some adsorbed molecules are able to “flip over”; they then exchange also the H atoms at the other side of the ring and leave the catalyst as C<sub>5</sub>D<sub>10</sub> molecules. A typical product pattern, as obtained with a conventional catalyst, is shown in Fig. 9.4. At low extent of exchange the pattern shows three predominant peaks, one at C<sub>5</sub>H<sub>9</sub>D<sub>1</sub>, one at C<sub>5</sub>H<sub>5</sub>D<sub>5</sub>, and one at C<sub>5</sub>D<sub>10</sub>. It is also known that multiple exchange of alkanes requires the ability of the molecule to form adsorption bonds through two vicinal C atoms, leading to H/D exchange of two H atoms positioned in  $\alpha$ – $\beta$  positions. That conclusion is based on the observation that the only alkane which shows negligible multiple exchange is neo-pentane, (CH<sub>3</sub>)<sub>4</sub>C, which contains 12 H atoms but no pair in  $\alpha$ – $\beta$  positions.

It is not exactly known how large a Pt<sub>n</sub> ensemble must be which can catalyze the multiple H/D exchange with D<sub>2</sub> of alkanes such as cyclopentane, but it stands to reason that at least two adjacent Pt atoms are required (probably more). It follows that a catalyst which has its Pt atoms predominantly isolated from each other should NOT show this product pattern, but give a product distribution typical of *stepwise* exchange. Such a product should follow the binomial law; i.e. no predominant peak at C<sub>5</sub>H<sub>5</sub>D<sub>5</sub>; the concentrations of the C<sub>5</sub>H<sub>10-x</sub>D<sub>x</sub> products at low exchange should show a monotonous decrease with  $x$ .

To test this hypothesis a Pt/mordenite catalyst was prepared from H-mordenite by exchanging a small amount of Pt and reducing at low temperature, so that Pt–H adducts could be formed and most Pt atoms were located in the *side pockets* of the

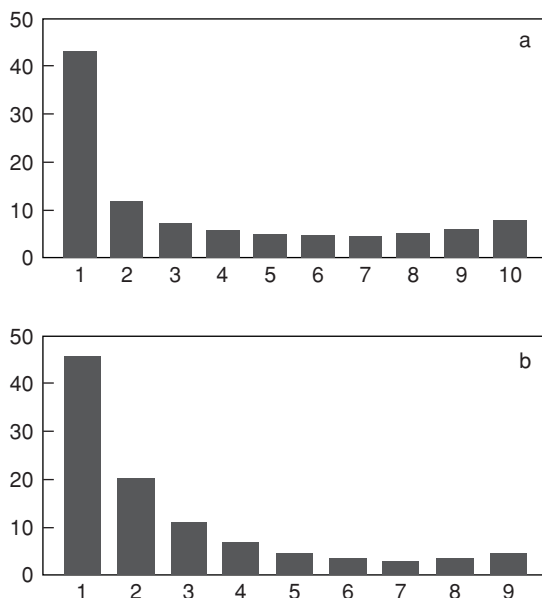


FIGURE 9.5. H/D stepwise exchange over Pt<sub>1</sub> in H-MOR. a. Cyclopentane b. Neopentane.

mordenite channels.<sup>30</sup> Exchange of cyclopentane with D<sub>2</sub> over this catalyst led to the product distribution shown in Fig. 9.5a.

Indeed, a monotonously decreasing abundance of exchanged molecules is found, peaks at  $x = 5$  and  $x = 10$  do not deviate from the pattern. For comparison the distribution of neo-pentane exchanged over the same catalyst is included in Fig. 9.5b. Both figures clearly show prevailing *stepwise* exchange. For neopentane this is typical because the molecule is lacking H pairs in  $\alpha - \beta$  position; for *cyclo*-pentane this result clearly indicates Pt sites that are different from those in all conventional catalysts which have been used in the numerous published studies of this exchange. The results indicate that in the Pt/H-mordenite catalyst as prepared and probed here, isolated Pt atoms, present as Pt-H<sup>+</sup> adducts, are the prevailing sites.

## 9.5. TRANSITION METAL OXIDES AND OXO-IONS

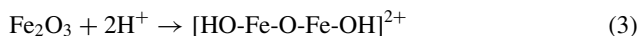
Most industrially desirable oxidation processes target products of partial, not total oxidation. Well-investigated examples are the oxidation of propane or propene to acrolein, butane to maleic acid anhydride, benzene to phenol, or the ammoxidation of propene to acrylonitrile. The mechanism of many reactions of this type is adequately described in terms of the Mars and van Krevelen model<sup>31</sup>: A molecule is chemisorbed at the surface of the oxide and reacts with one or more oxygen ions, lowering the electrochemical oxidation state of the metal ions in the process. After desorption of the product, the oxide reacts with O<sub>2</sub>, re-oxidizing the metal ions to their original oxidation state. The selectivity of the process is determined<sup>33</sup> by the relative chances of

a partially oxidized intermediate to either jump to the gas phase or react further with the oxide, finally leaving it as  $\text{CO}_2 + \text{H}_2\text{O}$ . Selectivity thus depends on the steepness of the curve relating the Gibbs Free Energy of removing oxygen from the solid to the extent of its reduction.<sup>33</sup> This gradient will depend on the size of the entity from which one or more oxygen atoms have to be removed. All other parameters being equal, this model leads us to expect that very small particles should be more selective oxidation catalysts than macroscopic oxides.

The selectivity for partial oxidation thus is basically controlled by the energy difference, for a given domain of the catalyst, to release either one oxygen atom rather than become deeply reduced. A small domain will release more easily one oxygen rather than a larger number, which would cause a very large change in oxidation number of the cations in the domain. Obviously, the domain size in small articles will be limited by the size of the oxide particle. The ability to release oxygen is not limited to neutral oxide particles, also oxo-ions such as  $\text{RhO}^+$  or  $[\text{HO-Fe-O-Fe-OH}]^{2+}$  can release part of their oxygen and thus act as active sites in catalytic oxidation. If linked to an appropriate support, their positive charge protects them against agglomeration.

An interesting variant of selective oxidation catalysis is the catalytic reduction of nitrogen oxides by ammonia or hydrocarbons. In this case the reducing molecule should specifically react with  $\text{NO}$  or  $\text{NO}_2$ , that are present in very low concentrations, rather than become oxidized to  $\text{CO}_2 + \text{H}_2\text{O}$  by reacting with  $\text{O}_2$  that is present in much higher concentration. The distinction between oxo-ions and oxide particle is most convenient if these entities are present on a zeolite support. Techniques have been developed to study the interconversion by IR spectroscopy:

- (a) agglomeration to large oxide particles by chemically neutralizing oxo cations,
- (b) redispersion of such oxide particles to oxo-ions by protons, e.g.



and registering the resulting change in catalytic performance, using the reduction of  $\text{NO}_x$  with *iso*-butane as the test reaction.

Work with the objective of comparing oxo-ions with oxide particles in order to test the validity of this reasoning has been reported by Chen *et al.* who used a catalyst that initially contains Fe oxo-ions,  $[\text{HO-Fe-O-Fe-OH}]^{2+}$ . These sites were first converted to  $\text{Fe}_2\text{O}_3$  particles by a simple chemical treatment. This was followed by another treatment, which redispersed these  $\text{Fe}_2\text{O}_3$  particles back to oxo-ions.<sup>34</sup> The change in particle size was monitored by a spectroscopic method based on the observation that in zeolites metal ions and oxo-ions, that are attached to the wall of a cage, give rise to a typical IR band caused by the perturbation of the vibrations of the zeolite lattice.<sup>35</sup>

In these tests, the  $\text{NO}_x$  was present in very low concentration and  $\text{O}_2$  in large excess. The “selectivity” is thus defined by the preference of the *iso*- $\text{C}_4$  for reducing the minority partner  $\text{NO}_x$  to  $\text{N}_2$  rather than the majority partner  $\text{O}_2$  to  $\text{CO}_2 + \text{H}_2\text{O}$ . In Fig. 9.6 the yield of  $\text{N}_2$  by reducing  $\text{NO}_x$  with *iso*-butane while increasing the temperature is depicted for an Fe/MFI catalyst treated in this manner. The curve of the highest yield is the original Fe/MFI catalyst exposing a high concentration of  $[\text{HO-Fe-O-Fe-OH}]^{2+}$  sites. The curve labeled Fe,Na/MFI shows the  $\text{N}_2$  yield after treating this catalyst with NaOH to induce agglomeration. As a result, the maximum  $\text{N}_2$  yield drops

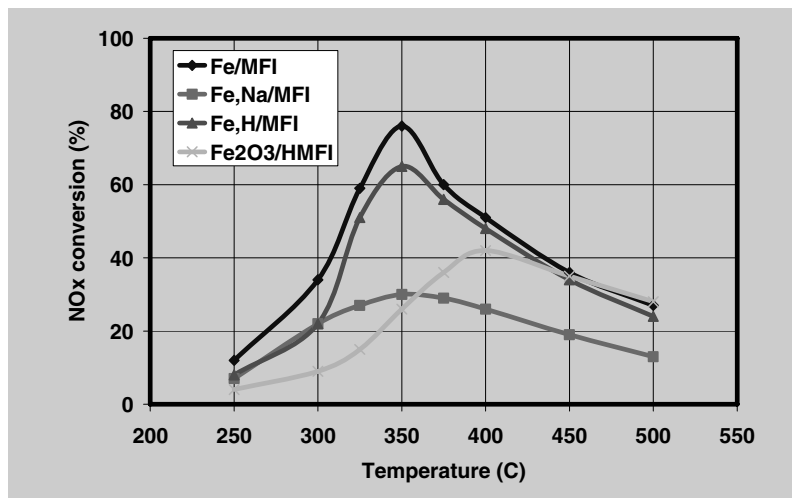


FIGURE 9.6.  $N_2$  yield of  $NO_x$  reduction with *iso*-butane over Fe/MFI in the presence of excess  $O_2$ . Fe/MFI: as prepared with large concentration of  $\{HO-Fe-O-Fe-OH\}$  ions. Fe, Na/MFI: same after NaOH treatment. Fe, H/MFI: same after exchanging  $Na^+$  against  $NH_4^+$  and transforming  $NH_4^+$  to  $H^+$ .  $Fe_2O_3$ /HMFI: catalyst prepared by incipient wetness impregnation of HMFI with Fe salt.

from 76% to 30%. The curve labeled Fe,H/MFI shows the  $N_2$  yield after exchanging the  $Na^+$  ions against  $NH_4^+$  ions and calcining it to regenerate the  $H^+$  sites. This treatment brings the  $N_2$  yield to 65%, i.e. almost back to the value over the original catalyst. The same graph also shows the  $N_2$  yield over another Fe/MFI catalyst with nearly the same Fe content that was prepared by impregnation and thus contained most of the iron as  $Fe_2O_3$  particles. Over this catalyst the maximum yield is only 26%. These results clearly demonstrate superior performance of oxo-ions over  $Fe_2O_3$  particles, though the size of the latter is still inside the nanoregime.

Another example of heterogeneous catalysis by oxo-ions is the one-step oxidation of benzene to phenol with nitrous oxide,  $N_2O$ . Fe/MFI catalysts have, again been found to be very active. This catalysis was discovered by Iwamoto<sup>36</sup> and has been extensively studied by the group of G. Panov in Novosibirsk.<sup>37–38</sup> Preparations of Fe/MFI which appear highly active for this reaction display poor activity for  $NO_x$  reduction and those which are optimum for that process, are poor for benzene oxidation. This shows that different sites are used. Work by Jia *et al.* revealed that the active sites for benzene oxidation appear to be Fe-oxo-ions containing only one Fe ion.<sup>39</sup> This does not necessarily mean that the sites are mononuclear. A recent work by Zhu *et al.* has rather suggested that the site consists of one  $Fe^{2+}$  and one  $Al^{3+}$  ion, the latter ion having left the zeolite framework.<sup>40</sup>

## 9.6. CONCLUSIONS

For metal catalysts used for hydrogenations and, in combination with acid functions, in hydrocarbon “reforming” reactions, the advantage of nano-size metal particles has been well known. More recently it has been demonstrated that metals on

the ascending branch of the “volcano shaped curves”, in particular gold, display high catalytic performance when present as nano-size particles on an appropriate support. With platinum it has been demonstrated that single atoms in zeolite cages are efficient sites displaying a catalytic activity that is distinctly different from that of multiatom particles exposing sites consisting of “ensembles.” For catalytic oxidations and reductions, recent work demonstrates the great advantages of fine-tuning the size of entities that consist of a small number of transition metal ions combined with oxide or hydroxide ions. Extremely high selectivity has been achieved with oxo-ions of Fe in the selective reduction of nitrogen oxides to N<sub>2</sub> and the one step oxidation of benzene to phenol.

## REFERENCES

1. H. Heinemann, Development of industrial catalysis, Handbook of Catalysis, edited by B. G. Ertl, H. Knözinger, and J. Weitkamp (Verlag Chemie, Weinheim) 1997, vol. 1, p. 35.
2. S. R. Blaszowski and R. A. van Santen, Quantum chemical studies of zeolite proton catalyzed reactions, *Top. Catal.* **4**, 145–156 (1997).
3. S. M. Csicsery, Shape selective catalysis in zeolites, *Zeolites* **4**, 202–213 (1984).
4. J. Jia, K. S. Pillai, and W. M. H. Sachtler, One-step oxidation of benzene to phenol with nitrous oxide over Fe/MFI catalysts, *J. Catal.* **221**, 119–126 (2004).
5. C. Remsburg and H. Higdon, Ideas for rent (UOP, Des Plaines, IL) (Publ) p. 259 (1994).
6. I. N. Stranski and R. Kaischew, Gleichgewichtsform und Wachstumsform der Kristalle, *Ann. Phys.* **21**, 330 (1935).
7. I. N. Stranski, Zur Berechnung der spezifischen Oberflächen-, Kanten-, und Eckenenergien an kleinen Kristallen, *Monatshefte Chem.* **69**, 234 (1936).
8. I. N. Stranski and R. Kaischew, Kristallwachstum und Kristallkeimbildung, *Phys. Zeitschr.* **36**, 393 (1936).
9. A. A. Balandin, Structural and energy factors in the theory of catalyst selection, *Sci. Select. Catal.* (1968).
10. J. Fahrenfort, L. L. van Reijen, and W. M. H. Sachtler, The decomposition of HCOOH on metal catalysts, *The Mechanism of Heterogeneous Catalysis* (Elsevier, Amsterdam) pp. 23–48 (1960).
11. W. M. H. Sachtler and J. F. Fahrenfort, Catalytic decomposition of HCOOH vapour on metals, *Actes du 2ième Congrès Intern. de Catalyse 1960*, (Editions Technip., Paris) pp. 831–863 (1961).
12. M. Haruta, Catalysis of gold nanoparticles deposited on metal oxides, *CatTech* **6**, 102 (2002).
13. A. A. Holscher and W. M. H. Sachtler, Chemisorption and surface corrosion in the tungsten + carbon monoxide system, as studied by field emission and field on microscopy, *Dis. Faraday Soc.* **41**, 29 (1966).
14. H. Topsøe, N. Topsøe, H. Bohlbro, and J. A. Dumesic, Supported iron catalysts: Particle size dependence of catalytic and chemisorptive properties, *Proc. 7th Int. Congress Catalysis*, edited by T. Seyama, K. Tanabe (Kondansha, Tokyo), p. 247 (1981).
15. S. M. Augustine and W. M. H. Sachtler, Catalytic probe for alloy formation in supported PtRe catalysts, *J. Catal.* **106**, 417–427 (1987).
16. S. M. Augustine and W. M. H. Sachtler, Variation of catalytic activity over PtRe/Al<sub>2</sub>O<sub>3</sub>, *J. Phys. Chem.* **91**, 5935–5956 (1987).
17. S. M. Augustine and W. M. H. Sachtler, On the mechanism for the platinum catalyzed reduction of rhenium in PtRe/γ-Al<sub>2</sub>O<sub>3</sub>, *J. Catal.* **116**, 184–194 (1989).
18. C. M. Tsang, S. M. Augustine, J. B. Butt, and W. M. H. Sachtler, Synthesis and characterization of bimetallic PtRe<sub>x</sub> clusters prepared by sublimation of Re<sub>2</sub>(CO)<sub>10</sub> onto Pt/NaY, *Appl. Catal.* **46**, 45–56 (1989).
19. Y. Z. Zhang, T. T. Wong, and W. M. H. Sachtler, The effect of Ca<sup>2+</sup> and Mg<sup>2+</sup> ions on the formation of electron-deficient palladium-proton adducts in zeolite, *J. Catal.* **128**, 13–22 (1991).

20. X. L. Bai and W. M. H. Sachtler, Methylcyclopentane conversion catalysis by zeolite encaged palladium clusters and palladium-proton adducts, *J. Catal.* **129**, 121–129 (1991).
21. T. J. McCarthy, G.-D. Lei, and W. M. H. Sachtler, Methylcyclopentane conversion catalysis over zeolite Y encaged rhodium; a test for the metal-proton adduct model, *J. Catal.* **159**, 90–98 (1996).
22. Z. C. Zhang, J. Hare, and B. Beard, Basicity of nanosized noble metal clusters in catalysis, 13th Int. Congr. Catalysis, Paris Abstract, 2-017 (2004).
23. Y. Z. Zhang, T. T. Wong, and W. M. H. Sachtler, The effect of  $\text{Ca}^{2+}$  and  $\text{Mg}^{2+}$  ions on the formation of electron-deficient palladium-proton adducts in zeolite, *J. Catal.* **128**, 13–22 (1991).
24. X. L. Bai and W. M. H. Sachtler, Methylcyclopentane conversion catalysis by zeolite encaged palladium clusters and palladium-proton adducts, *J. Catal.* **129**, 121–129 (1991).
25. T. J. McCarthy, G.-D. Lei, and W. M. H. Sachtler, Methylcyclopentane conversion catalysis over zeolite Y encaged rhodium; a test for the metal-proton adduct model, *J. Catal.* **159**, 90–98 (1996).
26. W. M. H. Sachtler and Z. Zhang, Zeolite supported transition metal catalysts, *Adv. Catal.* **39**, 129–220 (1993).
27. F. C. Gault, J. J. Rooney, and C. Kemball, Catalytic exchange with deuterium of polymethylcyclopentanes on metal films: Evidence for  $\pi$ -bonded intermediates, *J. Catal.* **1**, 225 (1962).
28. C. Kemball, The catalytic exchange of hydrocarbons with deuterium, *Adv. Catal.* **11**, 233 (1970).
29. R. L. Burwell, Jr., Use of deuterium on the study of heterogeneous catalysis, *Catal. Rev.* **7**, 25 (1972).
30. G.-D. Lei and W. M. H. Sachtler, H/D exchange of cyclopentane on Pt/mordenites: Probing for monoatomic Pt sites, *J. Catal.* **140**, 601–611 (1993).
31. P. Mars and D. W. van Krevelen, Oxidations carried out by means of vanadium oxide catalysts, *Chem. Eng. Sci. (Special Suppl.)* **3**, 41 (1954).
32. H.-Y. Chen, X. Wang, and W. M. H. Sachtler, Reduction of  $\text{NO}_x$  over zeolite MFI supported iron catalysts: Nature of active sites, *Phys. Chem., Chem. Phys.* **2**, 3083–3090 (2000).
33. W. M. H. Sachtler, G. J. H. Dorgelo, J. Fahrenfort, and R. J. H. Voorhoeve, Correlations between catalytic and thermodynamic parameters of transition metal oxides, *Proceedings 4th Int. Congress Catalysis*, Moscow, 1968 (Akad. Kiado, Budapest) vol 1971, pp. 454–465.
34. H.-Y. Chen, X. Wang, W. and W. M. H. Sachtler, Reduction of  $\text{NO}_x$  over zeolite MFI supported iron catalysts: nature of active sites, *Phys. Chem., Chem. Phys.* **2**, 3083–3090 (2000).
35. J. Sárkány and W. M. H. Sachtler, Redox chemistry of Cu/Na-ZSM-5; detection of cuprous ions by FTIR, *Zeolites* **14**, 7 (1994).
36. M. Iwamoto, K. Matsukami, and S. Kagawa, Catalytic oxidation by oxide radical ions. 1. One-step hydroxylation of benzene to phenol over group 5 or 6 oxides supported on silica gel, *J. Phys. Chem.* **87**, 903 (1983).
37. G. I. Panov, A. S. Kharitonov, and V. I. Sobolev, Oxidative hydroxylation using dinitrogen monoxide: a possible route for organic synthesis over zeolites, *Appl. Catal. A* **98**, 1 (1992).
38. G. I. Panov, A. K. Uriarte, M. A. Rodkin, and V. I. Sobolev, Generation of active oxygen species on solid surfaces. Opportunity for novel oxidation technologies over zeolites, *Catal. Today* **41**, 365 (1998).
39. J. Jia, K. S. Pillai, and W. M. H. Sachtler, One-step oxidation of benzene to phenol with nitrous oxide over Fe/MFI catalysts, *J. Catal.* **221**, 119–126 (2004).
40. Q. Zhu, R. M. van Teeffelen, R. A. van Santen, and E. J. M. Hensen, Effect of high-temperature treatment on Fe/ZSM-5 prepared by chemical vapor deposition of  $\text{FeCl}_3$ : II. Nitrous oxide decomposition, selective oxidation of benzene to phenol, selective reduction of nitrous oxide by *iso*-butane, *J. Catal.* **221**, 575–583 (2004).
41. R. Brill, E.-L. Richter, and E. Ruch, Adsorption of nitrogen on iron, *Angew. Chem. Int. Ed.* **6**, 882–883 (1967).